Light scattering and morphology of the lymphocyte as applied to flow cytometry for distinguishing healthy and infected individuals

Gennady I. Ruban
Vladimir V. Berdnik
National Academy of Sciences of Belarus
Stepanov Institute of Physics
Nezavisimosti Avenue 68
220072, Minsk, Belarus

Dmitry V. Marinitch
Natalia V. Goncharova
Centre of Hematology and Transfusiology
Ministry of Health of Belarus
Dolginovsky Ave. 160
223059, Minsk, Belarus

Valery A. Loiko
National Academy of Sciences of Belarus
Stepanov Institute of Physics
Nezavisimosti Avenue 68
220072, Minsk, Belarus

Abstract. A simple optical model of single lymphocytes with smooth and nonsmooth surfaces has been developed for healthy and infected individuals. The model can be used for rapid (in the real-time scale) solution of the inverse light-scattering problem on the basis of optical data measured by label-free flow cytometry. Light scattering patterns have been calculated for the model developed. It has been shown that the smooth and nonsmooth cells can be resolved using the intensities of the sideward- and backward-scattered light. We have found by calculations and validated by the flow cytometer experiments that intensity distributions for the cells of lymphocyte populations can be used as a preliminary signatures of some virus infections. Potential biomedical applications of the findings for label-free flow cytometry detection of individuals infected with viruses of hepatitises B or C and some others viruses are presented. © *2010 Society of Photo-Optical Instrumentation Engineers.* [DOI: 10.1117/1.3503404]

Keywords: lymphocyte model; light scattering; flow cytometry; virus infections.

Paper 10181RR received Apr. 7, 2010; revised manuscript received Aug. 17, 2010; accepted for publication Aug. 31, 2010; published online Nov. 2, 2010.

1 Introduction

Biological cells or other particles are characterized by a number of techniques.[1–7] Flow cytometry with ever-increasing applications in modern biomedical practice is among the much used methods.[8–10] This technique is based on single-particle analysis. It is extensively applied for the investigation of normal and pathological leukocytes by combining light scattering and immunophenotyping. The latter is a time-consuming process exploiting expensive monoclonal antibodies. In addition it uses cell labeling with fluorescence dyes, which are potentially toxic or interfere with normal cell functions.[11] Consequently, cell characterization through, mainly, scattering signals is of great interest because of potential reduction of operating costs and speeding up cell characterization as well as minimization or avoiding cell modification with dyes and antibodies. Conventional flow cytometry measures intensity of scattered light at two directions. Some advanced experimental devices, known as scanning (wide-angle) flow cytometers, measure angular dependences of intensity of scattered light ("cell fingerprints") over a wide interval of scattering angles.[1,12–15] Such flow-cytometric light-scattering patterns give new opportunities for characterization of normal and pathological cells.

To take advantage of these opportunities, one should be able to find a correlation between structures of scattered light and a scatterer. The correlation is obtained by light-scattering theory.[16–24] It retrieves the parameters of a single particle by solving an inverse light-scattering problem. To solve the inverse problem, optical models of a single scatterer are required. There are different models of single scatterers. Some of these models are very sketchy and take almost no account of cell structure. An example is the model of a homogeneous spherical particle.[23] The model includes a very limited number of parameters. Others models are cell-structure-oriented to a greater extent. An example is the model of a two-layer particle, which is more adequate. The leukocyte model is more complex and may include a variety of parameters,[25–27] in particular, refractive index[28–31] (the relative refractive index for leukocytes is in the range of about 1.01 to 1.08), cell shape and size, and nuclear shape and size. Biological cell models developed in the context of light-scattering problems as well as optical-scattering phenomena in cells and cellular organelles are the subject of wide speculation.[32–40]

The effect of scatterer surface morphology on light scattering is discussed with reference to different particles.[41–43] Recently, this effect has been examined also for biological cells.[34,44]

As noted earlier, we need have at hand a lymphocyte model that includes optical and morphometric components. The first component (refractive index distributions in cell constituents) is not always available at least in reliable, complete, and cell-specific form. The second component of the model is rather complex. It takes into consideration, for example, some nonsphericity of both the cell and its nucleus, quantitative data on an eccentric nucleus location and nucleus off-orientation within the cell,[26,27] cell surface texture,[34,44] and so on. To calculate the light-scattering pattern for a complex

Address all correspondence to: Gennady I. Ruban, National Academy of Science of Belarus, Stepanov Institute of Physics, Nezavisimosti Avenue 68, 220072, Minsk, Belarus. Tel: 375-17-2840797; Fax 375-17-2840879; E-mail: ruban@dragon.bas-net.by

model, one is forced to use complicated methods, for example, the finite difference time domain method (FDTD) and the discrete dipole approximation (DDA).[34,38] The previously mentioned deficiency of the initial optical data makes using the FDTD (and other complicated and precise methods) sometimes ineffective. In addition, as especially important in online applications, model complexity considerably decelerates calculations during cell discrimination by the solution of the inverse light-scattering problem. However, high rate analysis is essential for scanning flow cytometry. The recorded angular pattern has to be analyzed rapidly in a real-time scale on the order of milliseconds. That is why it is important to find some means to speed up the computer simulation during the cell characterization.

2 Problem Statement

One way to achieve this aim is to develop a cell model as simple as possible in the framework of a particular task. Such an approach avoiding the complex cell model enables us to characterize cells adequately only to the specificity of a particular biomedical task. However, for this specific task, we can characterize a cell quickly. Quickness can be achieved not only due to simplicity of a particular cell model, but due to respective simplification of methods of the inverse problem solving as well. So having at hand a particular biomedical task, it is reasonable to reveal the most prominent and simple feature of the cell as applied to the task.

As to a biomedical task, distinguishing of healthy and infected individuals is of great interest. To understand better the topicality of the task, it is helpful to mention that infections are ones of the most common diseases afflicting humans. For example, about 540 million people are chronically infected with hepatitis B and C worldwide.[45] In the United States, the number of people afflicted with hepatitis B and C per year makes up, respectively, 5 and 1.8% of the population (the data relate to 1988–1994).[46] Typically, it takes some years from the instance of the B, C virus infection to symptomatic chronic liver disease (cirrhosis and cancer); every carrier of the disease, whether symptomatic or not, is a potential source of infection to others.[45] Large-scale spreading of the specified virus infections (as well as of many other), their severe aftereffects for infected individuals themselves, and the eventuality of infecting people around them show that inexpensive and early recognition of individuals with virus infections is highly urgent.

As to a prominent and simple feature of the cell, we propose to distinguish healthy and infected individuals on the basis of surface structure of peripheral blood lymphocytes. We purposely pay attention to the structure of the lymphocyte surface. Our viewpoint is derived from the fact that the surface state of blood cells is responsible for a large variety of normal and pathological phenomena in healthy and afflicted persons.[47] Consider some data on the structure of a lymphocyte surface. The majority of peripheral blood lymphocytes of healthy individuals have a smooth surface; a smaller portion of peripheral blood lymphocytes is nonsmooth. Nonsmooth lymphocytes can be characterized by various features of the cellular surface structure. One of such surface structural features is microvilli, the small extended protrusions from the surface of a cell membrane. Microvilli can occupy the major-

ity of a lymphocyte surface.[48,49] Another surface structure feature is folds. There are also some other lymphocyte surface features. Lymphocyte populations actively respond to viruses in blood. For example, an analysis of the data in Ref. 47 shows that the ratio of percentage of smooth and nonsmooth lymphocytes (for instance, folded ones) is noticeably smaller for individuals with persistent hepatitis C virus as compared to healthy individuals. (It is worth noting that there are also data[47] on percentage changes of smooth and nonsmooth lymphocytes for individuals with persistent viruses of hepatitis B, tick-borne encephalitis, and herpes simplex as compared to healthy individual.)

So a potential candidate suitable for fulfilling a role of a prominent structure feature might be hypothetically identified as a surface structure of lymphocytes. Here, the following natural question appears, whether this hypothetical distinctive feature of cell morphology could be distinguished by a light-scattering pattern. If this is the case, then it seems reasonable to pose the task of distinguishing lymphocytes of infected individuals by the inverse light-scattering problem solution.

Having analyzed the morphological, optical, and biomededical aspects of the question, we put forward the following assumption: light-scattering patterns of cells with different surface structure features can be used as optical signatures of a normal or pathological status of lymphocyte populations in peripheral blood of individuals. To test this hypothesis, we constructed a simple model of lymphocytes of healthy and infected individuals. With this model, we calculate and analyze the angular patterns of light scattered by the modeling lymphocyte. The aim is to demonstrate that the non-smooth lymphocytes, for example, folded ones, can be distinguished from the smooth lymphocytes by cell light-scattering patterns without immunophenotyping (i.e., without using CD markers of the cells).

To our knowledge, modeling of cell morphology as applied to distinguishing lymphocyte populations of healthy and infected individuals has not yet been done. Simulation of the influence of surface cell structures on the cell light-scattering pattern for patients with persistent infections also is not investigated. This work is the first attempt to study some aspect of the problem. To develop a model of lymphocyte with near-surface features, we use, as a base, the findings of our paper in Ref. 27, as well as some known data. We adapt the known data to the problem involved and incorporated them into the model. The proper references to the original publications of known data are made. We present the experimental flow-cytometer data for lymphocytes of healthy and infected individuals to verify the model.

3 Materials and Methods

Cells of fresh peripheral blood are investigated in parallel for healthy and infected individuals (age 26 to 48 years). The experimental cycle of lymphocyte investigation includes cell study of one healthy and two infected individuals. Three cycles are made. A total of three healthy individuals and six infected individuals with persistent hepatitis C and hepatitis B with hepatic cirrhosis are examined. Hepatitis is diagnosed on the base of clinical presentation, ELIZA and PSR studies. The blood samples are obtained by venipuncture after informed consent of the individuals. The samples are placed in sterile

tubes containing preservative-free lithium heparin (20 U/ml), layered on a Ficoll-PaqueTM PLUS (1.077 g/cm³; GE Healthcare Bio-Sciences AB) and centrifuged at 300 g for 30 min at room temperature. The low-density mononuclear cells (MNCs) are accumulated at the Ficoll-Paque interface in accordance with their density. The accumulated cells are collected and washed twice in phosphate-buffered saline (PBS) containing 0.5% heat-inactivated embryonic calf serum (FCS; HyClone; Logan, Utah) and resuspended in PBS with 1% bovine serum albumin (BSA, Serva, Germany). Viability of the isolated cells is determined by a standard technique with the help of trypan blue stain (Sigma). The isolated MNC viability being tested with 500 to 600 cells for each individual is in the range from 98 to 100%. Final MNC concentration in suspension is about 1×10^6/ml.

Populations of isolated MNCs are determined by direct immunophenotyping. 5×10^5 cells are stained with monoclonal antibodies (mAbs) labeled with fluorescence dyes. FITS and PE are used as fluorescence dyes for the mAbs against CD14 (CALTAG) and CD45 (Beckman Coulter), respectively. MAbs are used at saturating concentrations. The staining is performed in 50 μl of PBS containing 1% BSA with the mAbs for 30 min at room temperature. To correct nonspecific staining of the cells, the reagents for blocking Fc-receptors are added to and mixed carefully with the samples. The samples are then washed twice with PBS containing 0.1% azide. For negative (isotypic) control, the cells are incubated with mouse immunoglobulin IgG$_1$ conjugated with FITS (IgG$_1$-FITS, Beckman Coulter) and PE (IgG$_1$-PE, CALTAG) for 30 min at room temperature and then washed twice by PBS with 0.1% azide.

Cell fluorescence and autofluorescence intensities are measured by flow cytometry using a FACScan instrument (Becton Dickinson). (To detect cell autofluorescence, the unstained MNCs are utilized.) Forward light scattering (FSC) and sideward light-scattering (SSC) intensities are also measured by FACScan. Next, the flow cytometry data are analyzed using the CellQuest software (Becton Dickinson). Populations of MNCs are determined after software logical gating of the lymphocytes on the basis of their FSC and SSC. The purity of lymphocyte population isolated for analysis is 94%. The number of the cells analyzed for each individual is 3×10^4.

4 Results and Discussion

In this section, we present a lymphocyte model and calculate its light-scattering pattern, aiming to distinguish between the lymphocyte populations of healthy individuals and persons suspected as being persistently infected by the viruses of hepatitises B or C, tick-borne encephalitis, or herpes simplex. The model developed takes into account the surface structure features of lymphocytes. In this section, we present the experimental flow-cytometer data for lymphocytes of healthy individuals and individuals with hepatitises B and C as well.

4.1 Lymphocyte Models and Calculated Light Scattering Patterns

We model lymphocytes by two-layer concentric spheres (Fig. 1). Such a model, unlike the simplest ones,[23] is more informative and, as distinct from complex models,[27] is suitable for rapid calculation in real time. The model ignores some struc-
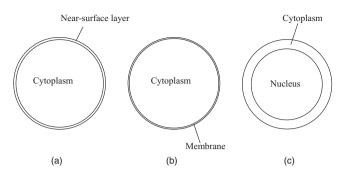

Fig. 1 Models of the lymphocytes with (a) nonsmooth and (b, c) smooth surfaces. Model (a) is developed in this paper for the cell with near-surface texture. Figures (b) and (c) display the known lymphocyte models with membrane (b) and nucleus (c). The cytoplasm, nucleus, and layer simulating cell texture are homogeneous. Cell parameters are indicated in Table 1.

ture features of lymphocytes. We will revert to reasonableness of our approximation later; for the moment, we proceed by describing the model. The nonsmooth surface of the cell is modeled by us as a homogeneous equivolume surface layer [see Fig. 1(a)]. Different thickness ranges of this layer simulate surface features of different kinds, such as, for example, folds and microvilli. The parameters of the cell model in our calculation are presented in Table 1 on the basis of our data[26,27] and known data.[50–61] Since surface changes of immunocompetent cells under persistent virus infections in question are nonspecific,[47] we suggest that cell and nucleus sizes and refractive indexes are the same for the healthy and afflicted individuals in question. The known models (cytoplasm–membrane and cytoplasm–nucleus) for a lymphocyte with smooth surface[50,51] are shown in Figs. 1(b) and 1(c). It is

Table 1 Cell parameters in our calculation of light scattered by the lymphocyte being in surrounding media with refractive index 1.35. Wavelength of the incident light is 0.63 μm.

Cell model components	Parameters	Values	Refs
Cytoplasm	Size, μm	7.5	26 and 27
	Refractive index	1.37	52 and 53
Nucleus	Size, μm	6.4	27
	Refractive index	1.39	54
Surface cell layer (simulating folds or villi)	Thickness, Folds μm	0.35	55
	Villi	0.05ᵃ	56, 57, and 61
	Refractive index	1.52	58–60 and refs. therein

ᵃThe value is estimated by us on the basis of data.[56,57,61] Note that the number density of villi is not the same on different lymphocytes. Therefore, it is necessary to vary the thicknesses of layers modeling villous surfaces for the different cells. Note also that there is a need to correct the layer thickness of given lymphocytes to take into account the fact that one part of the villous volume is occupied by cell membrane while the other part is occupied by cell cytoplasm having refractive index differing from that of the membrane. We estimate, on the base of the data in the cited references, that the corrected thickness is 0.05 μm for at least 65% of lymphocytes. Estimating the value 0.05 μm, we assume that 37.3% of villi volume is filled by membrane.
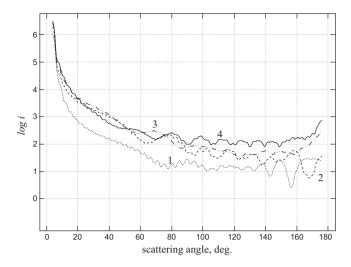
Fig. 2 Angular dependences of light-scattering intensity i calculated for a nonsmooth lymphocyte. Lymphocyte with microvilli (curve 1) and folds (curves 2, 3, and 4); thicknesses of the layers mimicking folds are 0.15 μm, 0.25 μm, and 0.35 μm, respectively; 40.7%, 69.6%, and 100% of fold volume is filled with membrane, respectively. Lymphocyte diameter corresponding to the typical value of lymphocyte size is 7.5 μm. Other cell parameters are indicated in Table 1.

Fig. 4 Angular dependences of light-scattering intensity i calculated for a lymphocyte at the left wing of the size distribution of the cells. Smooth lymphocyte (curve 1), nonsmooth lymphocyte with microvilli (curve 2) and folds (curves 3, 4, and 5); thicknesses of the layers mimicking folds are 0.15 μm, 0.25 μm, and 0.35 μm, respectively; 40.7%, 69.6%, and 100% of fold volume is filled with membrane, respectively. Lymphocyte diameter is 6.7 μm. Other cell parameters are indicated in Table 1.

worth noting that our designations "nonsmooth" and "smooth" are related to the cells rather than to the cell models.

The results of calculations for light-scattering patterns of model lymphocytes with nonsmooth and smooth surfaces [Figs. 1(a)–1(c)] are presented in Figs. 2 and 3, respectively. We used reliable high-accuracy, up-to-date code[62] to calculate intensities i^*. The value of $i^* = i_1^* + i_2^*$, where i_1^* and i_2^* are nondimensional intensities for light polarized parallel and orthogonal to the plane of scattering. Sometimes, i_1^* and i_2^* are referred as the Mie intensities. We averaged the calculated intensities i^* within a collection angle, taken as 7 deg. The

intensities averaged within this angle are denoted as i. (The same collection angle is used in the results displayed in Figs. 4–7). Comparison of the light-scattering patterns in Figs. 2 and 3 demonstrates that lymphocytes with surface features could be discriminated from smooth lymphocytes by the intensity differences. The intensity differences of light-scattering patterns for nonsmooth and smooth lymphocytes are mostly observed in the backward-scattered light, although some similar differences are seen in the forward-scattering
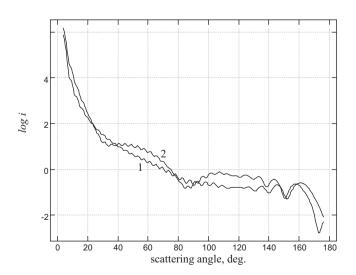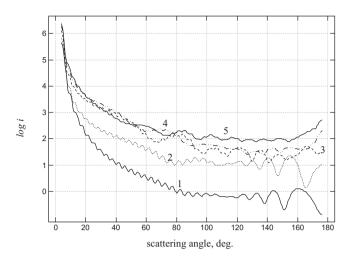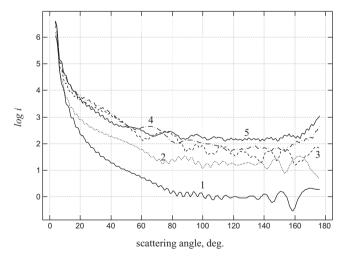

Fig. 3 Angular dependences of light-scattering intensity i calculated for the smooth lymphocyte; cell without (curve 1) and with (curve 2) nucleus. Lymphocyte diameter, membrane thickness, and refractive index are 7.5 μm, 10 nm, and 1.52, respectively. Other cell and nucleus parameters are indicated in Table 1.

Fig. 5 Angular dependences of light-scattering intensity i calculated for a lymphocyte at the right wing of the size distribution of the cells. Smooth lymphocyte (curve 1), nonsmooth lymphocyte with microvilli (curve 2) and folds (curves 3, 4, and 5); thicknesses of the layers mimicking folds are 0.15 μm, 0.25 μm, and 0.35 μm, respectively; 40.7%, 69.6%, and 100% of fold volume is filled with membrane, respectively. Lymphocyte diameter is 8.25 μm. Other cell parameters are indicated in Table 1.
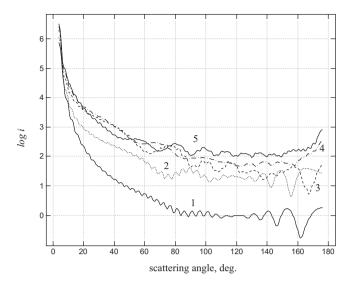
Fig. 6 Angular dependences of light-scattering intensity i calculated for a lymphocyte with membrane thickness of 11 nm. Smooth lymphocyte (curve 1), nonsmooth lymphocyte with microvilli (curve 2) and folds (curves 3, 4, and 5); thicknesses of the layers mimicking folds are 0.15 μm, 0.25 μm, and 0.35 μm, respectively; 40.7%, 69.6%, and 100% of fold volume is filled with membrane, respectively. Lymphocyte diameter is 7.5 μm. Other cell parameters are indicated in Table 1.

Fig. 7 Angular dependences of light-scattering intensity i calculated for a lymphocyte with membrane thickness of 9 nm. Smooth lymphocyte (curve 1), nonsmooth lymphocyte with microvilli (curve 2) and folds (curves 3, 4, and 5); thicknesses of the layers mimicking folds are 0.15 μm, 0.25 μm, and 0.35 μm, respectively; 40.7%, 69.6%, and 100% of fold volume is filled with membrane, respectively. Lymphocyte diameter is 7.5 μm. Other cell parameters are indicated in Table 1.

pattern as well. An angle range of scattering for finding the maximum intensity differences to distinguish the cells involved is 80 to 180 deg. This angular range is traceable with a scanning flow-cytometer; part of the range near 90 deg is traceable with the SSC-channel of a conventional flow-cytometer. Within the indicated angle range, the nonsmooth cells scatter light more strongly than the smooth cells, and the intensity of scattered light for nonsmooth and smooth lymphocytes roughly differs by at least a 1.1 order of magnitude. This difference is sufficient to be revealed, for instance, by light-scattering channels of a flow-cytometer, and in particular, by the SSC channel of a conventional flow-cytometer. On the basis of our calculations, we can anticipate comparative changes of SSC signal distributions for lymphocytes of infected and healthy individuals. Assume that the percentage of smooth lymphocytes is decreased and the percentage of non-smooth lymphocytes is increased, as happens with the cells of infected patients as compared to healthy individuals.[47] In this case, according to our calculations, the distribution will be shifted to large SSC signals for the infected individuals as compared with the healthy ones. Note that for near-backward directions, smooth cells scatter light more weakly than nonsmooth cells (see Figs. 2 and 3). This observation is in accordance with data.[34,43]

Therefore, smooth and nonsmooth lymphocytes are separated by differences in light-scattering intensity (see Figs. 2 and 3). Figures 2 and 3 show the results for typical values of lymphocyte size and membrane thickness. But the cells and their membranes have size variability, which can reduce the separation. Results of calculations taking into account the variability both of cell size and cell membrane thickness are presented in Figs. 4–7. One can see that there are still clear separations between the smooth and nonsmooth lymphocytes.
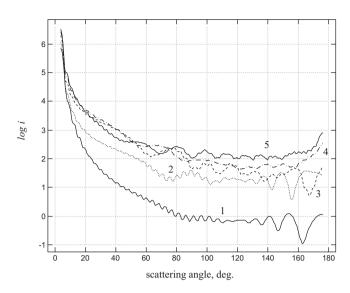
Aiming at a simple cell model, we neglect some structure features of the cells. In particular, we replace a slightly rough cell surface by an ideal spherical one. To determine the effect of such a replacement on particle light-scattering, we use the known literature data. The authors of paper in Ref. 34 compare calculated scattering patterns for the ideal sphere and a rough particle. The scattering patterns are computed by the FDTD method.[34] For these computations, (1) the optical parameters of the particles as well as the particle surroundings are similar to the ones in our calculations for lymphocytes, namely, diameters of the ideal and rough scatterers are 6 μm, scatterer refractive indices are 1.3675, and surrounding refractive index is 1.35; (2) the shape and roughness of the particle with rough surface are reconstructed from the 3-D confocal microscopy images of polystyrene particles. Now, assume that the roughness of the particle is analogous to one for the lymphocyte surface. Then, the rough particle and the ideal particle can be considered as an optical analog of the nonsmooth and smooth cell, respectively. The comparison of the scattering patterns for the ideal sphere and the rough particle shows that the mean intensity differences for these scatterers at the sideward and backward directions are less than 0.4 order of magnitude, while the differences of scattered light for models of nonsmooth and smooth lymphocytes are at least 1.1 order of magnitude. Hence, local roughness of the particle surface generating scatter in the fashion of very small Rayleigh scatterers does not move a central impact on the scattered intensity. It is worth noting that the authors of Ref. 34 also compare FDTD-calculated scattering patterns for the ideal sphere and a rough B-cell. Its shape and roughness is reconstructed from the 3-D confocal microscopy images for scattering pattern computation. Analysis of comparison data shows that the mean intensity differences for these scatterers are less than 0.5

order of the magnitude. These differences, in general, are large. Nevertheless, they are rather small in the context of the problem in question. Note that the small effect of roughness on angular scattering is also evident when comparing the light-scattering patterns calculated in paper Ref. 43 for the ideal sphere and Chebyshev particle being analog of rough particle. Thus, local roughness of the cell surface generating scatter in the fashion of very small Rayleigh scatterers does not have a dominant impact on scattered intensity. For the folded and villoused cells, the dominant impact for increased scattering is the thickness of the equivalent coated sphere.

Our lymphocyte model takes no notice of cell nucleus. Light-scattering patterns for cell models with and without a nucleus (Fig. 3) demonstrate that the maximal mean intensity difference is 0.4 order of magnitude. In the scattering angle range of about 85 to 95 deg, the difference is about 0.1 order of magnitude. Therefore, it is acceptable to ignore the nucleus in the lymphocyte model in the context of the problem involved. Generally speaking, a fairer comparison of cells with and without nucleus would be to correlate a membrane–cytoplasm in one case and a membrane–cytoplasm–nucleus in the other case. Nevertheless, provided that light-scattering-intensity is averaged in a large collection angle, the estimation being based on the results of Ref. 26 shows that the membrane contribution to the intensity for the sideward (80 to 100 deg) and backward (160 to 170 deg) directions of scattered light for lymphocytes is a rather small value (in the context of the problem). So, a nucleus-free model of lymphocytes is adequate in the frame of our biomedical task.

Our lymphocyte model takes no notice of such organelles as mitochondria and lysosomes, which can potentially contribute to the cell light scattering. The relative importance of organelles in light scattering is different in various cell types. Mitochondria play a significant role in light scattering for cells with high mitochondrial volume fraction,[63] especially for hepatocytes and some other cells, for instance, mammary tumor cell line EMT6.[36] Some types of cells have a significantly smaller volume fraction of mitochondria. As to lymphocytes, data on the number of mitochondria in these cells differ in various sources. It seems likely that the authors give data for different lymphocyte populations, including rare ones that are small in number. Data for the mitochondria contribution to lymphocyte light scattering are absent to our knowledge. For these cells one should, however, expect substantially smaller mitochondria contribution to light scattering than for hepatocytes or for other cells with high content of the mentioned organelles. The fact is that the number of mitochondria in lymphocytes is about 110 to 150 times smaller than in hepatocytes.[64] Lymphocytes contain a few mitochondria.[65] The mean amount of mitochondria in lymphocytes is 3.2 per cell.[66] So, it is reasonable to ignore mitochondria in the lymphocyte model. As for lysosomes, their contribution to cellular light scattering is noticeable for some cells with high content of these organelles. For EMT6, as an example of such cells, intensity of light scattered in the sideward direction for cells with lysosomes and cells without lysosomes (they are ablated by some procedure) is different by a 0.25 order of the value.[36] This difference being quite noticeable is nevertheless rather small in the context of the present paper. Lysosome contribution to lymphocyte light scattering will be even less than the previously mentioned value, because lymphocytes,
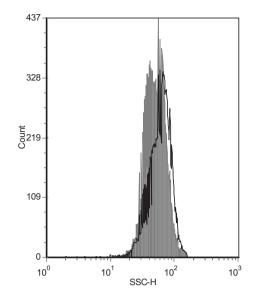

Fig. 8 Normalized histograms of the side-scattering signal distributions measured with FACScan flow cytometer and analyzed using CellQuest software (Becton Dickinson) for lymphocytes of a healthy individual (gray) and a patient with persistent hepatitis C (black).

excluding their small subpopulation as NK-cells, contain few lysosomes. For example, from the data in Refs. 67 and 68, lymphocytes contain only several lysosomes. Note, in our on-line task with millisecond calculations, we ignore the light-scattering influence of some organelles—in other words, we ignore certain homogeneity details of cell refractive index distribution. If long they computation is acceptable (off-line tasks with calculations, for example, by the DDA method), then the more realistic distribution of cell refractive index can be taken into account. The 3-D distributions of this kind are recently developed for some cells.[5] Calculations of the cell light-scattering patterns for large particles such as lymphocytes by DDA and similar methods is a separate complex task. Still, such methods give no opportunity to decrease time computation to obtain the real-time cell-distinguishing that is one of the main problem of scanning flow cytometry.

4.2 Experimental Data on Light-Scattering for Lymphocytes of Healthy and Infected Individuals

As mentioned earlier, intensity differences in light-scattering patterns calculated in the frame of the constructed model are sufficient to see contrast between the lymphocytes of healthy and infected individuals in the scattering angle range of 80 to 180 deg. Light scattered near the 90-deg scattering angle can be measured by the side-scattering (SSC) channel of a conventional flow-cytometer. We compare SSC signal distributions measured with a conventional flow-cytometer for cells of lymphocyte populations of healthy and infected individuals. The comparison, as exemplified in Figs. 8 and 9, shows that for infected individuals as compared with healthy ones, the distribution is shifted to large SSC intensities. (The distribution modification detected by the experiment reflects the lymphocyte population changes for infected individuals.) The experimental data support the results of our calculations for smooth and nonsmooth lymphocytes of healthy
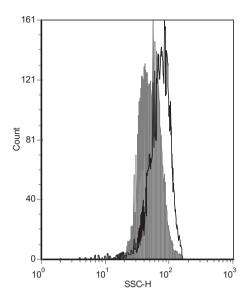
Fig. 9 Normalized histograms of the side-scattering signal distributions measured with FACScan flow cytometer and analyzed using CellQuest software (Becton Dickinson) for lymphocytes of a healthy individual (gray) and a patient with virus hepatitis B and hepatic cirrhosis (black).

and infected individuals. To understand the quantitative discrepancy between experimental and calculated data, one should take into account the following. Experimental data show scattering of cells for lymphocyte populations from healthy versus infected individuals. Calculated data show scattering of single smooth versus nonsmooth lymphocytes. Since both lymphocyte populations (of healthy and infected individuals) include both smooth and nonsmooth lymphocytes (and differ in their proportions; see Sec. 2), the discrepancy should exist. The less distinction in the proportion of smooth and nonsmooth cells between healthy and infected individuals, the more the discrepancy. It is worth noting that the shift of scattered intensity distribution for infected individuals as compared with healthy ones will be larger when measuring scattered light by scanning flow cytometer rather than by conventional instrument used in our experiment. The fact is that scattering intensity differences between smooth and nonsmooth lymphocytes are larger in the backward direction than in the sideward one. (Recall that measuring of scattering in the backward direction is accessible for the scanning instrument and inaccessible for the conventional one.) For example, the difference near the scattering angle 165 deg is about 4.5 times larger than the difference near the scattering angle 90 deg. Along with theoretical calculation, experimental results show that the indicated changes of the SSC signal distributions can be used as an additional parameter to be alert to a disease under primary detection of individuals infected with hepatitis B and C viruses. So our analysis demonstrates that scanning wide-angle flow-cytometers, being a new type of flow device, have a considerable quantitative advantage over the classic flow apparatus for the task we considered (distinguishing the lymphocyte populations of healthy and infected individuals without using cell CD markers).

As discussed earlier, flow-cytometers could detect infected individuals directly on the basis of the experimental data ex-

emplified in Figs. 8 and 9. To solve the task of this detection, we propose also a different mediated procedure with advanced facilities. It requires the lymphocyte model and involves solving the inverse problem on the basis of flow-cytometry light-scattering data. Solving the inverse problem enables one to distinguish (and to count the proportion of) smooth and nonsmooth cells in the lymphocyte population of an individual studied. For healthy versus infected individuals, the proportions are known to differ substantially. Additionally, for individuals infected by different viruses, the proportions also show marked distinctions.[47] Consequently, the individual proportions determined on the basis of solving the inverse light-scattering problem have potential importance as diagnostic and even differential diagnostic criterion. Note that the experimental data exemplified in Figs. 8 and 9 are best suited to screening rather than diagnostics. The proposed procedure based on the solution of the inverse light-scattering problem needs experimental validation. This is beyond the scope of this paper.

Thus, the findings show that the concentric homogeneous layer simulating lymphocyte surface texture (for example, cell surface folds) is necessary as the important constituent of the simple lymphocyte model with reference to the particular biomedical task involved. The layer simulating surface texture is applicable also as the constituent of our complex lymphocyte model[27] to extend and further develop it. As for the simple lymphocyte model in question, it can be used for rapid (in the real-time scale) solution of the inverse light-scattering problem on the basis of optical data measured by label-free flow cytometry. The proposed approach has another important application. It could be utilized to screen individuals of risk groups, by conventional or wide-angle flow-cytometer under the real-time mode, for detecting persons suspected as infected with some viruses.

5 Conclusion

A simple optical model of single lymphocytes with smooth and nonsmooth surfaces has been developed for healthy and infected individuals. This model can be used for rapid, in real-time scale, solution of the inverse light-scattering problem on the basis of optical data measured by label-free flow cytometry.

Angular patterns of scattered light have been calculated for the model constructed. Light scattering changes for lymphocyte populations of healthy individuals as compared to infected ones were examined by a conventional flow-cytometer. The experimental results validate the model constructed.

Calculations have demonstrated that the intensity differences of scattered light enable one to distinguish smooth and nonsmooth lymphocytes. The cells can be distinguished by the scattering intensities measured with a flow-cytometer in sideward and backward directions. Measuring of backward-scattered light with scanning flow cytometry gives more opportunities for distinguishing the cells as compared with using conventional flow cytometry, as the scattering intensity differences between smooth and nonsmooth lymphocytes in the backward direction are larger than in the sideward direction. For example, the difference at scattering angle 165 deg is about 4.5 times that at scattering angle 90 deg. The simulation is confirmed by the experiment data obtained with the

conventional flow-cytometer for lymphocyte populations of infected and healthy individuals. The intensity distributions can be used as preliminary signatures of some virus infections.

The findings show that it is possible to screen individuals of risk groups by immunophenotyping-free conventional or scanning flow cytometry for inexpensive and rapid provisional detecting of persons suspected as infected with viruses of hepatitises B and C, tick-borne encephalitis, and herpes simplex.

References

1. J.-L. Castagner and I. J. Bigio, "Particle sizing with a fast polar nephelometer," *Appl. Opt.* **46**, 527–532 (2007).
2. V. V. Tuchin, A. Tarnok, and V. P. Zharov, Eds., "Toward *in vivo* flow cytometry," *J. Biophoton.* **2**(8–9), 457–547 (2009).
3. Z. Du, K. H. Cheng, M. W. Vaughn, N. L. Collie, and L. S. Gollahon, "Recognition and capture of breast cancer cells using an antibody-based platform in a microelectromechanical systems device," *Biomed. Microdevices* **9**, 35–42 (2007).
4. E. I. Galanzha, M. S. Kokoska, E. V. Shashkov, J.-W. Kim, V. V. Tuchin, and V. P. Zharov, "*In vivo* fiber photoacoustic detection and photothermal purging of metastasis targeted by nanoparticles in sentinel lymph nodes at single cell level," *J. Biophotonics* **2**, 528–539 (2009).
5. W. Choi, C.-C. Yu, C. Fang-Yen, K. Badizadegan, R. R. Dasari, and M. S. Feld, "Field-based angle-resolved light-scattering study of single live cells," *Opt. Express* **33**(14), 1596–1598 (2008).
6. A. Wax and V. Backman, *Biomedical Applications of Light Scattering*, McGraw-Hill, New York (2009).
7. V. Backman, V. Gopal, M. Kalashnikov, K. Badizadegan, R. Gurjar, A. Wax, I. Georgakoudi, M. Mueller, C. Boone, R. Dasari, and M. Feld, "Measuring cellular structure at submicrometer scale with light scattering spectroscopy," *IEEE J. Sel. Top. Quantum Electron.* **7**(6), 887–893 (2001).
8. V. P. Zharov, E. I. Galanzha, E. V. Shashkov, N. G. Khlebtsov, and V. V. Tuchin, "*In vivo* photoacoustic flow cytometry for monitoring of circulating single cancer cells and contrast agents," *Opt. Lett.* **31**, 3623–3625 (2006).
9. J. L. Carey, J. P. McCoy, and D. F. Keren, *Flow Cytometry*, 4th ed., ASCP Press, Chicago (2007).
10. S. Sincock and J. Robinson, "Flow cytometric analysis of microorganisms," *Methods Cell Biol.* **64**, 511–537 (2001).
11. K. Katoh, K. Hammar, P. J. S. Smith, and R. Oldenbourg, "Birefringence imaging directly reveals architectural dynamics of filamentous actin in living growth cones," *Mol. Biol. Cell* **10**, 197–210 (1999).
12. K. Singh, X. Su, C. Liu, C. Capjack, W. Rozmus, and C. J. Backhouse, "A miniaturized wide angle 2D cytometer," *Cytometry* **69A**, 307–315 (2006).
13. V. Maltsev, "Scanning flow cytometry for individual particle analysis," *Rev. Sci. Instrum.* **71**, 243–255 (2000).
14. Y.-L. Pan, K. B. Aptowicz, R. K. Chang, M. Hart, and J. D. Eversole, "Characterizing and monitoring respiratory aerosols by light scattering," *Opt. Lett.* **28**, 589–591 (2003).
15. J. Neukammer, C. Gohlke, A. Hope, T. Wessel, and H. Rinneberg, "Angular distribution of light scattered by single biological cells and oriented particle agglomerates," *Appl. Opt.* **42**, 6388–6397 (2003).
16. Z. Ulanovsky, Z. Wang, P. Kaye, and I. Ludlov, "Application of neural networks to the inverse light scattering problem for spheres," *Appl. Opt.* **37**, 4027–4033 (1998).
17. P. M. Pilarski and C. J. Backhouse, "A method for cytometric image parameterization," *Opt. Express* **14**, 12720–12743 (2006).
18. K. Semyanov, P. Tarasov, A. Zharinov, A. Chernyshev, A. Hoekstra, and V. Maltsev, "Single particle sizing from light scattering by spectral decomposition," *Appl. Opt.* **43**, 5110–5115 (2004).
19. V. Berdnik and V. Loiko, "Particle sizing by multiangle lightscattering data using the high-order neural networks," *J. Quant. Spectrosc. Radiat. Transf.* **100**, 55–63 (2006).
20. A. Doicu, T. Wriedt, and Y. A. Eremin, *Light Scattering by Systems of Particles*, Springer-Verlag, Berlin (2006).
21. M. I. Mishchenko, L. D. Travis, and A. A. Lacis, *Multiple Scattering of Light by Particles: Radiative Transfer and Coherent Backscattering*, Cambridge University Press, Cambridge, UK (2006).
22. F. Borghese, P. Denti, and R. Saija, *Scattering from Model Nonspherical Particles. Theory and Application to Environmental Physics*, Springer, Berlin (2007).
23. V. P. Maltsev and K. A. Semyanov, *Characterization of Bio-Particles from Light Scattering*, Brill Academic Publishers, Boston (2004).
24. A. Hoekstra, V. Maltsev, and G. Videen, Eds., *Optics of Biological Particles, Nato Science Series, II, Mathematics, Physics, and Chemistry, II/238*, Springer, Dordrecht (2007).
25. F. Charriere, A. Marian, F. Montfort, J. Kuehn, and T. Colomb, "Cell refractive index tomography by digital holographic microscopy," *Opt. Lett.* **31**, 178–180 (2006).
26. G. I. Ruban, S. M. Kosmacheva, N. V. Goncharova, D. van Bockstaele, and V. A. Loiko "Investigation of morphometric parameters for granulocytes and lymphocytes as applied to a solution of direct and inverse light-scattering problems," *J. Biomed. Opt.* **12**, 044017 (2007).
27. V. A. Loiko, G. I. Ruban, O. A. Gritsai, A. D. Gruzdev, S. M. Kosmacheva, N. V. Goncharova, and A. A. Miskevich, "Morphometric model of lymphocyte as applied to scanning flow cytometry," *J. Quant. Spectrosc. Radiat. Transf.* **102**, 73–84 (2006).
28. V. V. Tuchin, *Tissue Optics: Light Scattering Methods and Instruments for Medical Diagnosis*, 2nd ed., SPIE Press, Bellingham, WA (2007).
29. F. A. Duck, *Physical Properties of Tissue: A Comprehensive Reference Book*, Academic Press, San Diego, CA (1990).
30. J. J. J. Dirckx, L. C. Kuypers, and W. F. Decraemer, "Refractive index of tissue measured with confocal microscopy," *J. Biomed. Opt.* **10**, 1–8 (2005).
31. J. M. Schmitt and G. Kumar, "Turbulent nature of refractive index variations in biological tissue," *Opt. Lett.* **21**, 1310–1312 (1996).
32. P. L. Gourley, J. K. Hendricks, A. E. McDonald, R. G. Copeland, K. E. Barrett, C. R. Gourley, K. K. Singh, and R. K. Naviaux, "Mitochondrial correlation microscopy and nanolaser spectroscopy—new tools for biophotonic detection of cancer in single cells," *Technol. Cancer Res. Treat.* **4**, 585–592 (2005).
33. D. Arifler, M. Guillaud, A. Carraro, A. Malpica, M. Follen, and R. Richards-Kortum, "Light scattering from normal and dysplastic cervical cells at different epithelial depths: finite-differences time domain modeling with a perfectly matched layer boundary condition," *J. Biomed. Opt.* **8**, 484–494 (2003).
34. R. S. Brock, X.-H. Hu, D. A. Weidner, J. R. Mourant, and J. Q. Lu, "Effect of detailed cell structure on light scattering distribution: FDTD study of a B-cell with 3-D structure constructed from confocal images," *J. Quant. Spectrosc. Radiat. Transf.* **102**, 25–36 (2006).
35. S. Tanev, W. Sun, J. Pond, V. V. Tuchin, and V. P. Zharov, "Flow cytometry with gold nanoparticles and their clusters as scattering contrast agents: FDTD simulation of light-cell interaction," *J. Biophoton.* **2**, 505–520 (2009).
36. J. D. Wilson and T. H. Foster, "Characterization of lysosomal contribution to whole-cell light scattering by organelle ablation," *J. Biomed. Opt.* **12**, 030503 (2007).
37. T. T. Wu, J. Y. Qu, and M. Xu, "Unified Mie and fractal scattering by biological cells and subcellullar structures," *Opt. Lett.* **32**, 2324–2326 (2007).
38. A. Karlsson, J. He, J. Swartling, and S. Andersson-Engels, "Numerical simulations of light scattering by red blood cells," *IEEE Trans. Biomed. Eng.* **52**, 13–18 (2005).
39. M. A. Yurkin, K. A. Semyanov, V. P. Maltsev, and A. G. Hoekstra, "Discrimination of granulocyte subtypes from light scattering: theoretical analysis using a granulated sphere model," *Opt. Express*, **15**, 16561–16580 (2007).
40. X. T. Su, C. Capjack, W. Rozmus, and C. Backhouse, "2D light scattering patterns of mitochondria in single cells," *Opt. Express* **15**, 10562 (2007).
41. G. Videen, Y. Shkuratov, E. Zubko, D. Petrov, W. Sun, T. Nousiainen, K. Muinonen, N. Voshchinnikov, and V. Illin, "Modelling irregular aerosols and their scattered light," in *Proc. 8th Conf. Electro-*

magnetic and Light Scattering by Nonspherical Particles: Theory, Measurements, and Applications, F. Moreno, J. J. Lopez-Moreno, O. Munoz, and A. Molinapp, eds., pp. 305–308 (2005).

42. T. Nousiainen and K. Muinonen, "Discrete dipole light scattering simulations for harmonic Gaussian particles," in *Ninth Conf. Electromagnetic and Light Scattering by Nonspherical Particles: Theory, Measurements, and Applications*, pp. 211–214 (2006).

43. D. Petrov, Y. Shkuratov, and G. Videen, "Analytical light-scattering solution for Chebyshev particles," *J. Opt. Soc. Am. A* **24**, 1103–1119 (2007).

44. I. V. Kolesnikova, S. V. Potapov, M. A. Yurkin, A. G. Hoekstra, V. P. Maltsev, and K. A. Semyanov, "Determination of volume, shape, and refractive index of individual blood platelets," *J. Quant. Spectrosc. Radiat. Transf.* **102**, 37–45 (2006).

45. G. Passi, "Safety of injections," *Indian Pediatr.* **37**, 345–347 (2000); available at http://www.indianpediatrics.net/march-345-350.htm.

46. M. J. Alter, D. Kruszin-Moran, O. V. Nainan, G. M. McQuillian, F. Gao, L. A. Moyer, R. A. Kaslov, and H. S. Margolis, "The prevalence of hepatitis virus infection in the United States, 1998 through 1994," *New England J. Medicine*, **341**, 556–562 (1999); available at http://digestive.niddk.nih.gov/statistics/statistics.htm.

47. I. O. Naslednicova, N. V. Riazantseva, V. V. Novitski, and M. A. Antoshina, "Changes of surface lymphocyte architectonics under chronic virus infection," *Tsitologiia* **47**, 136–140 (2005; in Russian).

48. J.-L. Carpentier, E. van Obberghen, P. Gorden, and L. Orci, "Surface redistribution of ^{125}I-insulin in cultured human lymphocytes," *J. Cell Biol.* **91**, 17–25 (1981).

49. D. Kenney, L. Cairns, E. Remold-O'Donnell, J. Peterson, F. S. Rosen, and R. Parkman, "Morphological abnormalities in the lymphocytes of patients with the Wiskott-Aldrich syndrome," *Blood* **68**, 1329–1332 (1986).

50. R. A. Meyer, "Light scattering from biological cells: dependence of backscatter radiation on membrane thickness and refractive index," *Appl. Opt.* **18**, 585–588 (1979).

51. A. Brunsting and P. F. Mullaney, "Light scattering from coated spheres: model for biological cells," *Appl. Opt.* **11**(3), 675–680 (1972).

52. M. Kohl and M. Cope, "Influence of glucose concentration on light scattering in tissue," *Opt. Lett.* **17**, 2170–2172 (1994).

53. F. Lanni, A. S. Waggoner, and D. L. Taylor, "Structural organization of interphase 3T3 fibroblasts studied by total internal reflection fluorescence microscopy," *J. Cell Biol.* **100**, 1091–1102 (1985).

54. A. Brunsting and P. Mullaney, "Differencial light scattering from spherical mammalian cells," *Biophys. J.* **14**, 439–453 (1974).

55. G. W. Schmid-Schonbein, Y. Y. Shih, and S. Chien, "Morphometry of human leukocytes," *Blood* **56**, 866–875 (1980).

56. C. C. Hoffmann, K. C. Moore, C.-Y. Shih, and R. L. Blakley, "Scanning electron microscopy of human lymphocytes during transformation and subsequent treatment with methotrexate," *J. Cell. Sci.* **28**, 151–165 (1977).

57. S. Majstoravich, J. Zhang, S. Nicholson-Dykstra, S. Linder, W. Friedrich, K. A. Siminovitch, and H. N. Higgs, "Lymphocyte microvilli are dynamic, actin-dependent structures that do not require Wiskott-Aldrich syndrome protein for their morphology," *Blood* **104**, 1396–1403 (2004).

58. M. D'Arienzo, A. Doria, G. Gallerano, E. Giovenale, and A. Orlando, "Studies on cell membrane functionality: an experimental setup for liposome exposure," (2002) available at http://www.frascati.enea.it/t...ns/Posters/Tu-P22-Darienzo.ppt.

59. C. Jones and K. Suhling, "Refractive index sensing using fluorescence lifetime imaging," *J. Phys.: Conf. Ser.* **45**, 223–230 (2006).

60. S. Johnsen and E. A. Widder, "The physical basis of transparency in biological tissue: ultrastructure and the minimization of light scattering," *J. Theor. Biol.* **199**, 181–198 (1999).

61. G. I. Kozinets, V. M. Pogorelov, D. A. Shmarov, S. F. Boev, and V. V. Sazonov, *Blood Cells—Modern Technology of Analysis*, Triada-Pharm, Moscow (2002; in Russian).

62. V. A. Babenko, L. G. Astafyeva, and V. N. Kuzmin, *Electromagnetic Scattering in Disperse Media: Inhomogeneous and Anisotropic Particles*, Springer-Praxis, Berlin (2003).

63. R. Drezek, M. Guillaud, T. Collier, I. Boiko, A. Malpica, C. Macaulay, M. Follen, and R. Richards-Kortum, "Light scattering from cervical cells throughout neoplastic progression: influence of nuclear morphology DNA content and chromatin texture," *J. Biomed. Opt.* **8**(1), 7–16 (2003).

64. X. Jing, "Establishment of a two-dimensional electrophoresis map of human mitochondrial proteins," available at http://edoc.hu-berlin.de/dissertation/xie-jing-2003-12-15/HTML/chapter5.html (2003).

65. P. Heywood, "Evidence from serial sections that some cells contain large numbers of mitochondria," *J. Cell. Sci.* **26**, 1–8 (1977).

66. G. Nagy, M. Barcza, N. Gonchoroff, P. E. Philips, and A. Perl, "Nitric oxide-dependent mitochondrial biogenesis generate Ca2+ signalling profile of lupus T cells," *J. Immunol.* **173**(6), 3676–3683 (2004).

67. Y. Sadahira, K. Akisada, T. Sugihara, S. Hata, K. Uehira, N. Muraki, and T. Manabe, "Comparative ultrastructural study of cytotoxic granules in nasal natural killer cell lymphoma, intestinal T-cell lymphoma, and anaplastic large cell lymphoma," *Virchows Arch.* **438**, 280–288 (2000).

68. G. Brittinger, R. Hirschhorn, K. Hirschhorn, and G. Weissmann, "Effect of pokeweed mitogen on lymphocyte lysosomes," *J. Cell Biol.* **40**, 843–846 (1969).